Dipolar and contact processes in H_2 o-p conversion on ionic surfaces

1993 J. Phys.: Condens. Matter 5 7325

(http://iopscience.iop.org/0953-8984/5/40/008)

J. Phys.: Condens. Matter 5 (1993) 7325–7342. Printed in the UK

Dipolar and contact processes in H_2 o–p conversion on ionic surfaces

K Makoshi†, M Rami and E Ilisca

Laboratoire de Magnétisme des Surfaces, Université Paris 7, 2 place Jussieu, 75251 Paris Cédex 05, France

Received 10 May 1993, in final form 14 July 1993

Abstract. Different channels in the *ortho–para* conversion of hydrogen molecules physisorbed on a transition metal oxide surface are investigated. The Wigner process, which assumes catalysts to be point dipoles, is analysed and compared to the dipolar and contact processes, which include the orbital degrees of freedom of the surface electrons. Three possible ground states, corresponding to different surface structures, are considered and their relative efficiencies discussed. In particular, the o–p conversion rate is found to be very sensitive to the presence of a metal dangling bond perpendicular to the surface. The molecule–metal electron overlap is shown to strengthen the contact process considerably but the dipolar one only negligibly. Our general expressions are illustrated by a simple model, corresponding qualitatively to chromium impurities dispersed on an alumina surface and discussed in terms of two parameters: the surface–molecule distance d, and the effective metal nuclear charge Z. A fluctuation of about 100% in the o–p conversion rates, when compared to the original Wigner theory, is found.

1. Introduction

This paper deals with the theoretical analysis of some elementary (one-step) channels of the *ortho–para* conversion of hydrogen molecules physisorbed on a transition metal oxide.

All the past experimental studies of o–p H_2 conversion on magnetic surfaces have been analysed in terms of the Wigner model, originally derived in 1933 [1]. Astonishingly, the underlying assumptions of this model, essentially catalyst magnetic point dipoles, have never been discussed. The numerous discrepancies between the experimental measurements of the o–p H_2 conversion rate on ionic surfaces and the Wigner theoretical model have been recently reviewed [2]. As the experimental rates can exceed the theoretical ones by more than an order of magnitude [3, 4], we found it necessary to examine properly the usual assumption of catalyst magnetic point dipoles.

We investigate, in this paper, a few elementary 'one-step' channels: the dipolar D and contact Y ones, in which we take explicitly into account the orbital degrees of freedom of the surface electrons. For each channel, three levels of analysis of decreasing generality are proposed. (a) The conversion algebra, based on group theory, allows us to express the conversion rates in terms of orbital tensors, functions of the surface electron configuration. (b) These tensors are expressed in terms of surface orbitals and illustrated by considering three 3d electrons of metal cations corresponding qualitatively to chromium impurities diluted at the surface of an alumina substrate. The extension of the formalism to an arbitrary number of orbitals is straightforward. (c) In order to obtain qualitative estimates in terms of

† Permanent address: Faculty of Engineering Science, Osaka University, Toyonaka, Osaka 560, Japan.

0953-8984/93/407325+18$07.50

a reduced number of parameters, a simple hydrogenoid form for the radial 3d wavefunction is inserted in the general expressions. This allows analytical expressions of the matrix elements and numerical estimates in terms of only two parameters: d, the Cr–molecule distance and Z, the effective ionic charge of Cr.

At low temperature, the H_2 molecule is assumed to be adsorbed at a distance d from the Cr^{3+} ion on the symmetry axis perpendicular to the surface lattice plane. On pure alumina, the H_2 molecule was found to be adsorbed on the top of an interstitial aluminium ion or vacancy, at a distance $d = 2.4$ Å $\simeq 4.54$ a.u. above the oxygen plane and rather insensitive to the presence or absence of an Al^{3+} interstitial ion [5]. The surface 'cluster' is assumed to be of C_{4v} symmetry. A simple geometry could be the bipyramid H_2–MO_5, where the Cr^{3+} ion M = Cr^{3+} ($3d^3$) is surrounded by five oxygen ions at equal distances and on the three axes, with the H_2 on the top. Larger clusters of different symmetries are also possible, but there is great advantage in using the basis functions (ξ, η), ζ, u and v of the representations e, b_2, a_1 and b_1 of the C_{4v} group. The same basis functions span the cubic group. These are the usual combinations of the 3d radial part and harmonic orientations. (Calculations on lower, or higher, symmetries can be derived from this basis.) We then include the inter-electron Coulomb interaction by constructing the triple products which are irreducible representations of C_{4v}. The new three-electron 3d basis functions are obtained as linear combinations of (3×3) Slater determinants, constructed from the original spin orbitals ξ, η, ..., and eigenfunctions of S^2 and S_z where S represents the total electron spin momentum [6]. The quadruplets are known to lie lower than the doublets, because of exchange interaction, and we restrict our considerations to the former. For the MO_5 geometry, the quadruplet $(e^2b_2)^4B_1$ is most certainly the ground state since it cumulates all the advantages of strong exchange, π bonding with the O ions and high crystal-field splittings. However, when the O ion below the metal one is missing, we obtain the MO_4 geometry where the axial orbital $u = d_{z^2}$ of representation a_1 becomes a dangling bond competitive with the others. In this case $(a_1e^2)^4A_2$, and $(a_1eb_2)^4E$ with orbital degeneracy, are equally possible candidates. Our purpose is to express the different conversion rates in terms of the orbital basis $(\xi, \eta, u, \ldots)$ and illustrate their sensitivities to different inter-electron couplings identified by their symbols ${}^4\Gamma = {}^4B_1, {}^4A_2, {}^4E$. (Appendix A lists a few of their eigenfunctions.)

The molecule's nuclear system is composed of the rotational system, of eigenstates Y_m^L and eigenenergies $E_L = \frac{1}{2}\hbar\omega_{op}L(L+1)$, and the spin system. Defining the nuclear spins $I(a)$ and $I(b)$ at the protons a and b, the total momentum $I = I(a) + I(b)$ has the eigenvalue zero in the *para* states and one in the *ortho* states. Due to Pauli antisymmetrization they are associated with the even and odd rotational states respectively. However we shall only retain in the following the first *o–p* transition connecting the *para* state defined by $|p\rangle = |L = I = 0\rangle$, together with the first *ortho* one, defined by $|o_{II}\rangle = |L = I = 1, m_l, m_i\rangle$, since this is the preponderent one at low temperatures. Moreover, at higher temperatures, the other *o–p* transitions, ΔL odd, can be expressed in terms of it by multiplying by a temperature dependent factor.

The *o–p* transition rate, inside the manifold ${}^{2S+1}\Gamma$, is obtained from time dependent perturbation theory as

$$P_{o\to p}({}^{2S+1}\Gamma) = \frac{1}{\hbar^2}\sum_{\gamma\gamma' mm'} p_{\gamma,m}\sum_{i,I}|\langle {}^{2S+1}\Gamma, \gamma', m', p|H|{}^{2S+1}\Gamma, \gamma, m, o_{II}\rangle|^2 J(\omega_{op}) \qquad (1.1)$$

where γ, m and γ', m' define the initial and final electron orbital and spin substates respectively with initial probability occupation $p_{\gamma,m} = p_\gamma p_m = [{}^{2S+1}\Gamma]^{-1}$, since we neglect

spin–orbit splittings ([ ] denotes the state degeneracy). $J(\omega_{op})$ represents the spectral density of molecular motion at the *o–p* frequency $\omega_{op} = 3.54 \times 10^{12}$ s^{-1}. Different models have been suggested to describe $J(\omega_{op})$, owing to the catalyst substrate and the conditions of pressure and temperature at the surface [7, 8].

The hyperfine Hamiltonian H couples the electron and nuclear degrees of freedom. The physical picture is that the inhomogeneous magnetic field, arising from the surface electronic spins, uncouples the molecule nuclear spins. Therefore only the antisymmetric part, with respect to proton interchange, is retained in the interaction. In the physisorption regime, each proton being much closer to the molecule centre than to the surface electrons, the magnetic field difference is fairly well approximated by the field gradients.

The dipolar processes $\boldsymbol{W}$ and $\boldsymbol{D}$ are considered in section 2. We give first a modern (condensed) version of Wigner's theory. It assumes a catalyst magnetic dipole located at the cation site. In the oxides considered here, when the orbital momentum is quenched, this arises from the total electron spin. Because of its simplicity, the Wigner process, denoted $\boldsymbol{W}$, has been used by all experimentalists to interpret their data. Then, we enlarge the formalism to incorporate the orbital degrees of freedom of the catalyst electrons and obtain the $\boldsymbol{D}$ process, for different possible ground states. Section 3 details the hyperfine contact processes. The simple contact of the d electron with the H_2 proton is denoted by $\boldsymbol{Y}$, while the overlap induced contact process is denoted by $\boldsymbol{OY}$. Using the metal–molecule electron antisymmetrization allows some intramolecular electron–proton contact. The different processes are then compared and discussed. Some concluding comments are given in section 4, while the details of the algebra and analytical calculations are reported in the appendices.

2. The dipolar process

The dipolar coupling, hereafter denoted $\boldsymbol{D}$, arises from the antisymmetric part of the double dipole–dipole interaction between the electron spins and the two nuclear spins $\boldsymbol{I}$(a) and $\boldsymbol{I}$(b) of the hydrogen protons a and b. The dipolar Hamiltonian can be written as

$$\boldsymbol{D} = \lambda_d \sum_{\alpha} [\boldsymbol{s}^1(\alpha) \times \boldsymbol{i}^1]^2 \cdot [\boldsymbol{T}^2(\alpha a) - \boldsymbol{T}^2(\alpha b)] \tag{2.1}$$

where $\lambda_d = 1.571 \times 10^{-7}$ a.u., $\boldsymbol{s}(\alpha)$ is the spin momentum of electron α, $\boldsymbol{i} = \boldsymbol{I}(a) - \boldsymbol{I}(b)$ the molecule nuclear spin difference and $\boldsymbol{T}^k(r) = \boldsymbol{Y}^k(\theta, \phi)/r^{k+1}$, αa (respectively αb) being the distance vector between the electron α and the proton a (respectively b). In the following ab denotes the internuclear vector. (Tensors in the spherical basis are used throughout the paper [9].) By performing a limited series expansion around the molecule centre of mass, applying the gradient formula and using the recoupling properties of four angular momenta, the dipolar Hamiltonian (2.1) can be re-written in a simpler form

$$\boldsymbol{D} = \lambda_d \sqrt{15} \boldsymbol{N}^2 \cdot \boldsymbol{E}^2 \tag{2.2}$$

where the nuclear tensor (denoted $\boldsymbol{N}$ for nucleus)

$$\boldsymbol{N}^2 = (\boldsymbol{i}^1 \times \boldsymbol{ab}^1)^2 \tag{2.3}$$

pertains to the nuclear spin and rotational degrees of freedom, inducing the o–p transitions with selection rules $\Delta I = \Delta L = 1$, whereas the electron tensor (denoted E for electron)

$$E^2 = \sum_{\alpha} E^2(\alpha) \tag{2.4}$$

$$= \sum_{\alpha} [T^3(\alpha) \times s^1(\alpha)]^2 \tag{2.5}$$

operates on the spin and position degrees of freedom (relative to the molecule centre) of the electron α, with the position tensor defined as $T^3 = Y^3(r)/r^4$.

The essential assumption of Wigner considers the magnetic impurity as a point dipole, located in heterogeneous conversion, on a surface site. In this approximation, the electron matrix elements are found to obey the following simple sum rule:

$$\sum_{m,m',\beta} (-)^{\beta} p_m \langle m'|E^2_{-\beta}|m\rangle\langle m|E^2_{\beta}|m'\rangle = \frac{5}{12\pi} S(S+1) d^{-8}. \tag{2.6}$$

The nuclear matrix elements are simply worked out, leading to

$$\sum_{i,l} \langle p|N^2_{-\nu}|o_{il}\rangle\langle o_{il}|N^2_{\beta}|p\rangle = (-)^{\beta}\delta_{\beta,\nu}\frac{ab^2}{3}. \tag{2.7}$$

Inserting (2.6) and (2.7) in (1.1), the transition rate is written as

$$P^W_{o\to p} = k d^{-8}. \tag{2.8}$$

The temperature factor, also denoted the Wigner constant

$$k = (25/12\pi)(\lambda_d ab/\hbar)^2 S(S+1) J(\omega_{op}) \tag{2.9}$$

contains the contributions from the electron spins, the molecular rotation and spin of the nuclei, as well as the temperature dependent spectral density of the thermal motion at the surface. When d is expressed in a.u., the Wigner constant k is expressed in s^{-1}. For a Cr^{3+} impurity of spin $S = \frac{3}{2}$, k amounts to $\sim 2 \times 10^8$ s^{-1} when $J(\omega_{op})$ is taken, at room temperature, to be of the order of the molecule–impurity contact time $\simeq 10^{-12}$ s. The o–p rate is found to be proportional to μ^2/d^8 (μ represents here the impurity magnetic moment), which is referred in the literature as the Wigner law. (The original law was in fact derived in the gas phase, where Wigner related the interaction time t to the approach distance d through $t = (d/3v)$, v being the thermal velocity, which brings the rate $\simeq d^{-6}$. This does not however apply to a catalyst surface.) We remark that, in this formalism, the impurity magnetic moment arises solely from the total electron spin and the conversion rate becomes identical for different electron configurations. At room temperature, and at a distance $d = 4.5$ a.u., the conversion time $\tau_{o\to p} = (P_{o\to p})^{-1}$ is roughly of the order of 1 ms, while at liquid nitrogen temperature $\tau_{o\to p} \simeq 1$ mn and at very low temperature $\tau_{o\to p} \simeq 1$ h.

We take now into account the surface electrons' orbital degrees of freedom. The resulting conversion rate can be written in a form similar to (2.8):

$$P^D_{o\to p}(\Gamma) = k K^D(\Gamma) \tag{2.10}$$

where $K^D(\Gamma)$, being defined by (B1), represents an effective average $\langle r^{-8}\rangle_\Gamma$ over the electron orbitals which span the representation Γ. In the case of a non-degenerate ground state Γ, it is shown in appendix B that $K(\Gamma)$ has the form of a scalar product

$$K^D(\Gamma) = [4\pi/7(\times 9)]\boldsymbol{T}^3(\Gamma)\cdot\boldsymbol{T}^3(\Gamma) \tag{2.11}$$

of tensors $\boldsymbol{T}^3(\Gamma) = \sum_\omega \boldsymbol{T}^3(\omega)$, which sum the different tensorial matrix elements $\boldsymbol{T}^3(\omega) = \langle\omega|\boldsymbol{T}^3|\omega\rangle$, over the orbitals ω. For ${}^4\Gamma = {}^4B_1$, $\omega = \xi, \eta, \zeta$ while for ${}^4\Gamma = {}^4A_2$, $\omega = u, \xi, \eta$. In terms of the 3d orbital angular momentum eigenstates $|2, n\rangle$, and using the simplified notation $\langle R_{3d}Y^2_{n'}|T^3_\alpha|R_{3d}Y^2_n\rangle = \langle n'|\alpha|n\rangle$ for the matrix elements, we obtain the conversion rates

$$P^D_{o\to p}({}^4B_1) = k[4\pi/(7\times 9)][2\langle 1|0|1\rangle + \langle 2|0|2\rangle]^2 \tag{2.12}$$

$$P^D_{o\to p}({}^4A_2) = k[4\pi/(7\times 9)][2\langle 1|0|1\rangle + \langle 0|0|0\rangle]^2. \tag{2.13}$$

For the degenerate manifold ${}^4E$, (2.11) must be replaced by (B6) with $(\gamma, \gamma') = (\xi, \eta)$, introducing the non-diagonal elements $\langle\xi|\boldsymbol{T}^3|\eta\rangle\cdot\langle\eta|\boldsymbol{T}^3|\xi\rangle$, and leading to the conversion rate

$$P^D_{o\to p}({}^4E) = k\frac{4\pi}{7\times 9}\left[\left|\sum_{m=0,1,2}\langle m|0|m\rangle\right|^2 + |\langle 1|2|-1\rangle\right|^2\Bigg]. \tag{2.14}$$

When the effect of the molecule–Cr electron overlap is included, the wavefunction u must be replaced by $N_{gu}[u - g\langle a\rangle\langle g|u\rangle]$ where $N_{gu} = [1 - \langle g|u\rangle^2]^{-1/2}$, and the matrix element $\langle 0|0|0\rangle$ that appears in (2.13) and (2.14) is replaced by $N^2_{gu}[\langle 0|0|0\rangle - 2\langle g|0\rangle\langle 0|0|g\rangle]$. The explicit calculation of $\langle 0|0|g\rangle$ shows that this matrix element remains very small except at very short distances, which would correspond to H_2 chemisorption, for which our model is not valid. We can therefore conclude that the dipolar processes are not directly modified by metal–molecule non-orthogonality effects. (The chemisorption well minimum is located below 2 a.u. whereas the physisorption one is above 4 a.u.; in between is an energy barrier. In the physisorption regime, the metal–molecule electron overlap characterizes rather well the admixture of states since it corresponds roughly to the ratio of the metal–molecule electron repulsion divided by the energy difference between the metal and molecule electron ground states. For small values of the overlap, say smaller than 0.3, a simple first-order orthogonalization procedure is thus sufficient to describe the admixture.)

The relative efficiencies of the dipolar mechanism corresponding to the electron eigenstates ${}^4\Gamma = {}^4B_1$, ${}^4A_2$ and ${}^4E$ are compared to the Wigner one in figure 1, as a function of the distance d, for $Z = 4.8$. We have plotted, in figure 2, the orbital averages $P^D_{o\to p}({}^4\Gamma)/P^W_{o\to p} = \langle(r/d)^{-8}\rangle_\Gamma$, as a function of the nuclear charge Z, for $d = 4.5$ a.u. It is first apparent that for long surface–molecule distances d, we recover the Wigner rate in d^{-8}. But at the usual distances of adsorption ($d = 4.5$ a.u.) many powers of d are operative, as well as exponential decreases, arising from the Cr orbitals. The most efficient dipolar channels are those which contain the dangling bond u: ${}^4A_2$ and ${}^4E$. Among them, the ${}^4A_2$ channel is faster since it contains the orbitals (ξ, η) which point in planes perpendicular to the surface, whereas the ${}^4E$ channel contains the in-plane orbital ζ. Finally the ${}^4B_1$ channel, containing the orbitals ξ, η and ζ remains weaker. At $d = 4.5$ a.u. and $Z = 4.8$, the ${}^4A_2$ and ${}^4E$ dipolar channels exceed the Wigner one by 41% and 21% respectively, while the ${}^4B_1$ one is 63% smaller. It is therefore clear that the conversion efficiency increases

when the three-electron ground state contains orbitals with larger metal–molecule electron overlap. However, the analysis in terms of the orbitals' spatial extension, measured in our model by the parameter Z as represented in figure 2, is more complex. We must recall that the conversion process arises from the catalyst magnetic field gradients. When Z is small the orbitals are rather diffuse and the electron spread decreases these gradients. Therefore increasing values of Z increase the surface field inhomogeneity and the conversion rates. In contrast when Z is large, since the electrons are more concentrated around their nucleus, the electron probability amplitude at the molecule decreases sharply with increasing values of Z. For large Z this intensity decrease overcomes the influence of the magnetic inhomogeneity for the channels $^4A_2$ and ^4E which contain the dangling bond u but not for the $^4B_1$ one. The $^4A_2$ and ^4E conversion rates pass thus through a maximum at $Z = 5.8$ and 5.3 respectively increasing the Wigner rate by about 60% and 30%. All rates converge towards the Wigner one for very large values of Z, as expected for a point magnetic dipole. It is remarkable that the dipolar processes become almost vanishing for $Z < 3$, as seen in figure 2.

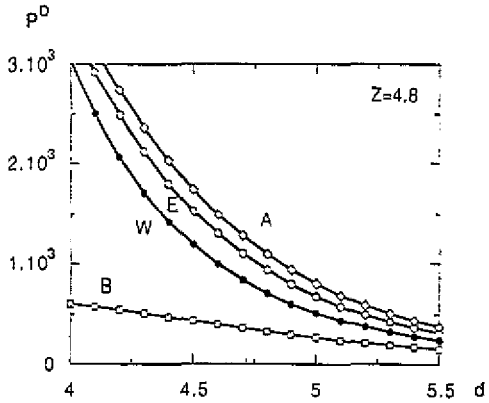

Figure 1. The dipolar conversion rates $P^D_{o\to p}(\Gamma)$ (in s^{-1}), corresponding to the channels $^4\Gamma = B(^4B_1)$, $A(^4A_2)$ and $E(^4E)$, are represented as a function of the Cr–molecule distance d (in a.u.), for $Z = 4.8$, and compared to the Wigner one $P^W_{o\to p}$.

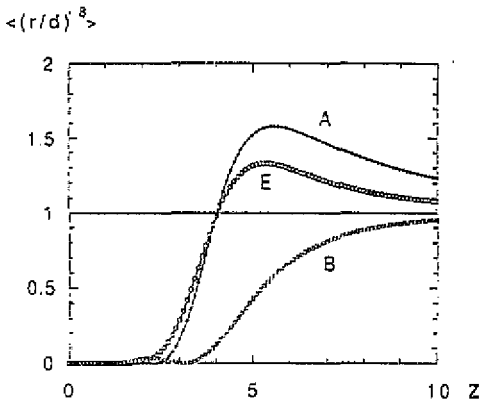

Figure 2. The orbital averages $P^D_{o\to p}(^4\Gamma)/P^W_{o\to p} = \langle(r/d)^{-8}\rangle_\Gamma$, corresponding to the channels $^4\Gamma = B(^4B_1)$, $A(^4A_2)$ and $E(^4E)$, are represented as a function of the nuclear charge Z, for $d = 4.5$ a.u.

We conclude that the Wigner assumption of a point dipole leads to only an average conversion rate for H_2 molecules adsorbed on a transition metal oxide surface. The surface electronic configuration must therefore be analysed in detail to interpret the strength of the dipolar interactions with the adsorbed molecules. Before considering the contact processes, it is interesting to notice that when the electron eigenstate does not have the maximum spin multiplicity but has identical orbital basis, a different orbital form factor is found in the conversion rate. For instance, for $(e^2b_2)^2B_1$ we find

$$P^D_{o\to p}(^2B_1) = k[4\pi/(7\times 9)][4\langle 1|0|1\rangle - \langle 2|0|2\rangle]^2 \tag{2.15}$$

where k is still given by (2.9) with $S = 1/2$. Although at long distances (2.15) converges towards the Wigner rate (2.8), at shorter distances it has a different structure from (2.8) and (2.12).

3. The contact processes

The antisymmetric part (with respect to proton interchange) of the hyperfine contact coupling between the spins of the electrons and the nuclei leads to the Hamiltonian

$$Y = \lambda_c i^1 \cdot \sum_\alpha s^1(\alpha)[\delta(\alpha a) - \delta(\alpha b)] \tag{3.1}$$

where αa (αb) is the distance vector between the electron α and the proton a (b), $s(\alpha)$ is the spin momentum of electron α and $i = I(a) - I(b)$ the molecule nuclear spin difference. $\delta(r)$ represents the Dirac operator and $\lambda_c = \lambda_d(5\pi)^{1/2}(\frac{2}{3})^{3/2} = 3.39 \times 10^{-7}$ a.u.

The calculation of the contact induced conversion probability parallels the dipolar one, the major difference arising from the orbital operator. The usual first-order expansion of the Dirac operators, around the molecular centre M, gives

$$\delta(\alpha a) - \delta(\alpha b) = ba^1 \cdot \nabla^1 \delta(\alpha M) = -(2i/\hbar) a b^1 \cdot \delta(\alpha M) p^1 \tag{3.2}$$

which introduces the momentum operator. Inserting this in (3.1), and restricting to a spin manifold S, which allows us to substitute $s^1(\alpha)$ by $S^1 = \sum_\alpha s^1(\alpha)$ multiplied by the ratio q_s of their reduced matrix elements (for the states of maximum spin, here considered, q_s is equal to the inverse of the number of d electrons):

$$Y = -\frac{2i}{\hbar}\lambda_c q_s [i^1 \cdot S^1]\left[ab^1 \cdot \sum_\alpha \delta(\alpha M) p^1\right]. \tag{3.3}$$

Recoupling the four momenta, the contact Hamiltonian (3.1) can be re-written in simpler form

$$Y = \lambda_c \sum_{h=0,1,2} (-)^h N^h \cdot E^h \tag{3.4}$$

where, as precedingly, we have disentangled the nuclear operator

$$N^h = (i^1 \times ab^1)^h \tag{3.5}$$

inducing the o–p transitions, from the electron one

$$E^h = -\frac{2iq_s}{\hbar}\left(S^1 \times \sum_\alpha \delta(\alpha M) p^1\right)^h. \tag{3.6}$$

It is shown in appendix B, that the o–p conversion rate, relative to the hyperfine contact process Y, defined by (3.4)–(3.6), and induced by the catalyst electrons in a $^{2S+1}\Gamma$ eigenstate, can be written in the condensed form similar to (2.8) and (2.10)

$$P^Y_{o\to p}(\Gamma) = kK^Y(\Gamma) \tag{3.7}$$

where k denotes the Wigner constant (2.9).

In the case of a non-degenerate orbital ground state Γ, the contributions from the electron orbitals have again the form of a scalar product:

$$K^Y(\Gamma) = [2^7/(3^3 \times 5)](\pi q_s)^2\{\Theta^1(\Gamma) \cdot \Theta^1(\Gamma)\} \tag{3.8}$$

where $\Theta^1(\Gamma)$ contains the sum, over the orbitals ω which span Γ, of the operator $(i/\hbar)\delta(\alpha M)p^1$ matrix elements and is simply expressed, in terms of one electron orbitals, as

$$\Theta^1(\Gamma) = \frac{i}{\hbar}\sum_{\omega}\langle\omega|\delta(\alpha M)p^1|\omega\rangle = \sum_{\omega}[\omega\nabla^1\omega](M) \tag{3.9}$$

where M denotes the position of the molecule centre, relative to the metal nucleus C. The orbitals ω and their gradients are thus estimated at M: CM = d.

In the case of a degenerate ground state Γ, the orbital contributions contain non-diagonal extra terms:

$$K^Y(\Gamma) = \frac{2^7}{3^3\times 5}(\pi q_s)^2\sum_{\gamma,\gamma'} p_\gamma \Theta^1(\gamma,\gamma')\cdot\Theta^1(\gamma',\gamma) \tag{3.10}$$

where the three-electron matrix elements of the operator $\Theta^1 = \sum_\alpha \delta(\alpha M)p^1$, denoted by $\Theta^1(\gamma,\gamma') = \langle\Gamma,\gamma|\Theta^1|\Gamma,\gamma'\rangle$, can be reduced to one-electron ones.

However, these general formulae become much simpler in the particular geometry considered here. When the H_2 molecule is assumed to be adsorbed at a distance d from the metal ion, on the symmetry axis perpendicular to the surface lattice plane, the amplitudes of the metal orbitals $\omega = \xi, \eta, \zeta$ vanishing on this axis, the contact induced conversion cannot occur in the case of a $^4B_1$ ground state: $K^Y(^4B_1) = 0$. In the cases of the $^4A_2$ and ^4E ground states, the orbital form factors become equal and the summation over the orbitals ω in (3.9) and (3.10) is reduced to only one contribution arising from the dangling bond $\omega = u$. The calculations, detailed in appendix B.2, lead to the following expression in terms of the parameters Z and d:

$$K^Y(^4A_2) = K^Y(^4E) = [2^9/(3^{25}\times 5)]Z^{14}d^6(Zd-6)^2\exp(-\tfrac{4}{3}Zd). \tag{3.11}$$

We now study the effect of the molecule–Cr electron overlap. The contact-induced conversion probability keeps the formal structure defined by (3.7), (3.8) and (3.10), but a new orbital operator must be defined by

$$\Theta^1(\Gamma) = \sum_{\omega} N_{g\omega}[\omega(M) - g(a)S_{g\omega}]\nabla^1\omega(M) \tag{3.12}$$

where $S_{g\omega} = \langle g|\omega\rangle$ denote the different overlaps of the one-electron orbitals ω, which span Γ, with the molecular one g, and $N_{g\omega} = (1 - S_{g\omega}^2)^{1/2}$. Because of our first-order expansion, the catalyst electron orbitals and their gradients are both taken at the molecule centre, whereas g is taken at the proton, since $g(a) = g(b)$. The amplitude of the molecular electron bonding orbital at the nuclear spins, is modulated by the molecule–catalyst electron overlaps. The wavefunction u being replaced by $[u - g(a)\langle g|u\rangle][1-\langle g|u\rangle^2]^{-1/2}$, the resulting o–p conversion rates, relative to the overlap contact process OY in the $^4A_2$ channel, are obtained as

$$P^{OY}_{o\to p}(^4A_2)/P^{Y}_{o\to p}(^4A_2) = [u - g(a)\langle g|u\rangle]^2/u^2(d)[1-\langle g|u\rangle^2] \tag{3.13}$$

and similarly for the ^4E ones. $P^{Y}_{o\to p}(^4A_2)$ is given by (3.7) and (3.11). As before, the overlap contact induced conversion cannot occur in the case of a $^4B_1$ ground state: $K^{OY}(^4B_1) = 0$. We have represented $P^{OY}_{o\to p}(^4A_2)$, and compared it with $P^{Y}_{o\to p}(^4A_2)$ in figure 3 as a function

of distance d, for $Z = 4.8$, and in figure 4 as a function of Z, for $d = 4.5$ a.u. The ratio (3.13) is represented as a function of Z, for $d = 4.5$ a.u., in figure 5. It is apparent from these figures that the overlap contact process $\boldsymbol{OY}$ is much larger than the simple contact one $\boldsymbol{Y}$, by about one order of magnitude. The direct contact process appears to be weaker than the dipolar ones, except for very small Z ($Z < 3$) where the metal orbitals are rather diffuse. The overlap contact process becomes more efficient than the dipolar ones, for $Z < 4.3$. It is essentially dominated by the amplitude of the metal orbital at the molecule centre, as well as by the molecule–metal overlap. The importance of the surface electron distribution inhomogeneity is manifested through the increase of the ratio (3.13) with Z, whereas the $\boldsymbol{Y}$ and $\boldsymbol{OY}$ rates decrease with increasing Z. The amplitude strength thus overcomes the gradient strength more clearly in the contact processes than in the dipolar ones. In other words, the maximum that may appear in the dipolar rates appears in the contact ones, shifted towards much lower Z values. At $Z = 3$ the $\boldsymbol{OY}$ process becomes the most efficient one. Its rate exceeds that of the $\boldsymbol{D}$ process by a factor of ~ 13. We obtain a factor of four when comparing to the $\boldsymbol{D}$ rate maximum at $Z = 5.8$. Moreover the contact processes decrease more slowly than the dipolar ones, with increasing surface–molecule distance d. Because of the Cr–molecule electron overlap, the electrons cannot be distinguished and a Cr electron may reach an H proton through a molecular orbital. This mixing of the catalyst 3d electrons with the molecular ones shifts the range of the contact interaction to larger distances and thus strengthens the o–p conversion rate [10]. A similar overlap mechanism was considered in 1972 [11], and found to be efficient in the analysis of chemical shifts in paramagnetic mixtures.

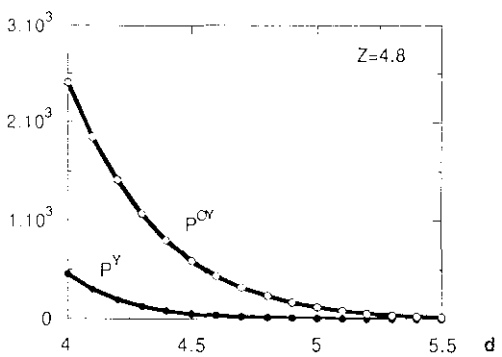

Figure 3. The contact conversion rates $P^{\boldsymbol{Y}}_{o\to p}(\Gamma)$ and $P^{\boldsymbol{OY}}_{o\to p}(\Gamma)$ (in s^{-1}), corresponding to the channels $^4\Gamma$ = $A(^4A_2)$ or $E(^4E)$, are represented as a function of the Cr–molecule distance d (in a.u.), for $Z = 4.8$.

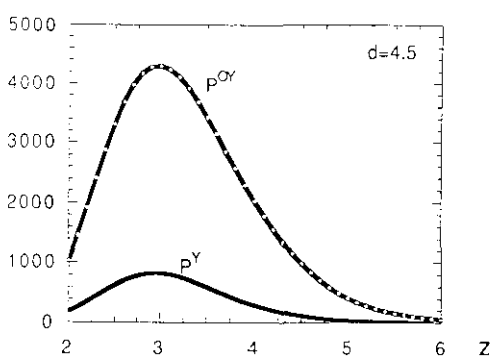

Figure 4. The contact conversion rates $P^{\boldsymbol{Y}}_{o\to p}(\Gamma)$ and $P^{\boldsymbol{OY}}_{o\to p}(\Gamma)$ (in s^{-1}), corresponding to the channels $^4\Gamma$ = $A(^4A_2)$ or $E(^4E)$, are represented as a function of the nuclear charge Z, for $d = 4.5$ a.u.

Summarizing, we have shown for all the processes investigated that the conversion rate is very sensitive to the surface orbital basis which spans the many-electron ground state. In particular the presence of dangling bonds that point perpendicularly to the catalyst surface, and therefore have stronger electron overlaps with the molecules, strengthens the conversion rate. The maximum efficiency is obtained when some balance is reached between the two contradictory requirements of strong surface metal electron amplitudes and their gradients. The dipolar processes are found to be faster for large Z ($Z > 4.5$), associated with localized

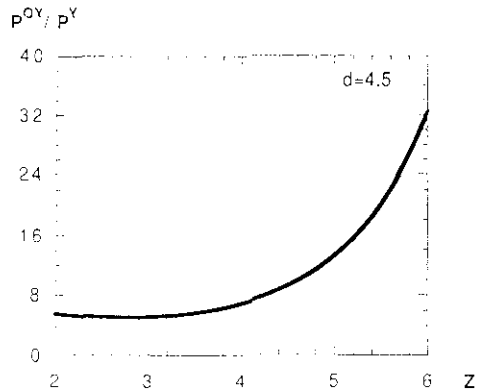

Figure 5. The ratio of the contact conversion rates $P^{OY}_{o\to p}(^4\Gamma)/P^{Y}_{o\to p}(^4\Gamma)$, corresponding to the channels $^4\Gamma = A(^4A_2)$ or $E(^4E)$, are represented as a function of the nuclear charge Z, for $d = 4.5$ a.u.

electrons and strong surface magnetic gradients. In contrast the contact processes become the faster ones for smaller Z ($Z < 4$), associated with delocalized electrons and strong electron amplitudes at the adsorbed molecules. These results show that o–p conversion measurements might give important complementary information on the surface metal degree of ionicity and on the influence of surface pretreatments.

4. Concluding comments

The processes described above focus on one-step hyperfine interactions, where the H nuclear spins are under the direct influence of the surface electrons. The two-step mechanisms, where these hyperfine interactions are modulated by the surface molecule Coulomb interactions, as described briefly in [12], will be detailed in a forthcoming publication. By considering the electron orbital degrees of freedom we have obtained higher or lower conversion rate estimates than those obtained within Wigner's model, depending on the surface electron configuration symmetries and radial extensions.

Our argument is rather simple. The different metal electrons occupy orbitals which are differently orientated in space. Consequently, the hyperfine interactions with an adsorbed H_2 molecule are very sensitive to the orbital geometry. The orbital degrees of freedom of the surface electrons selectively modulate the o–p conversion rate and must therefore be considered. In particular the metal–molecule electron antisymmetrization introduces non-diagonal effects which are proportional to the electron overlap. We have considered here contact and dipolar interactions, and diagonal as well as non-diagonal effects, on a surface structure characterized by a transition metal ion surrounded by ligands of tetragonal symmetry. In the processes investigated we have merely concentrated on the surface–molecule distance and the effective metal ionic charge dependences.

The distance dependences of the mechanisms depicted appear quite different from the simple 'd^{-8}' Wigner's law. The consideration of the surface electron distribution, in the dipolar interaction with the H nuclear spins, adds many other powers of d, as well as exponential decreases of comparable magnitudes. The dipolar mechanism is found to be only slightly affected by the electron overlap. In contrast, this overlap enhances the contact

mechanism by about one order of magnitude, making this process faster than the dipolar one when strong covalent bonds are established between the transition metal and the O ions, spreading the metal electrons. However in that case, our estimates must be modulated by the O admixtures. A calculation including the respective influence of the O on the conversion rate is under consideration. In the case of ionic surfaces, the dipolar process, being of longer range, increases and becomes faster than the contact one. It must also be noticed that the overlap contact process is more sensitive to the orientation of the surface electron orbitals than the dipolar process. At room temperature for instance, the molecules being mobile along the surface, we are expecting a decrease of the axial contribution, whereas the electrons distributed along the vertical planes will overcome the axial decrease and enhance the contact processes. The decomposition of the conversion rate into different orbital contributions therefore becomes temperature dependent.

The model chosen to represent the electron surface configuration is rather simplified. We have omitted configuration mixing, and spin–orbit interaction and taken into account the covalent bonds with the O ions in a crude fashion. Moreover the H_2 adsorption kinetics are concentrated within a single spectral density. The corresponding estimates of the absolute conversion rates are therefore approximate.

Much theoretical work remains to be done, in order to extract from conversion measurements useful information about electronic configurations on surfaces of metal oxides. Our formalism can easily be extended to a variety of geometrical symmetries and different n-electron couplings. Then the covalent mixing of the transition metal impurity with the O ions should be described by more accurate wave functions, which take into account self-consistently the amplitudes of admixture and the respective spatial extensions.

On the experimental side, low temperature measurements on clean surfaces are difficult presently because of low resolution. 'o–p' conversion rates could however be measured down to 77 K. At these temperatures, the H_2 molecules at the surface are continuously renewed and it is rather simple to analyse the gas sample composition. Despite the fact that surface–gas phase exchange and surface mobility can now be rather well modelled, we do not think that the fitting of absolute conversion rates in terms of a significant number of parameters would be useful. Rather we think that the comparisons of o–p rates performed with one kind of impurity dispersed on different substrates, or different impurities dispersed on the same substrate, would be much more meaningful.

Summarizing, we have shown that the surface electrons' orbital degrees of freedom play an important role in the H_2 o–p conversion process. The Wigner model used up to now by all experimentalists and almost all theoreticians is found, in many cases, to be too weak, and at best very approximate, whenever applied to a realistic surface configuration.

Acknowledgments

One of the authors (KM) acknowledges Université Paris 7 for inviting him and all members of Laboratoire de Magnétisme des Surfaces for their hospitality during his stay in Paris.

Appendix A. Electron eigenstates

Although the following model can easily be extended to a variety of ionic surfaces, we chose to illustrate the processes investigated on a particular surface configuration. We consider that the O ions form a square lattice, with a Cr ion at the centre. One O ion may lie below, or not, depending on the surface.

The free Cr d electron wavefunctions are taken as $|2, n\rangle = R_{3d}Y_n^2$, where $R_{3d} = N_{3d}r^2\exp(-\frac{1}{3}Zr)$, $N_{3d} = (2^3/3^9 \times 5)^{1/2}Z^{7/2}$. Z denotes the effective nuclear charge of Cr^{3+} and can be estimated from 'Slater rules' as a difference between the atomic number Z_0 of the free ion minus a screening constant S [13]. If we retain only the shielding of the Cr inner shells, we obtain $Z = 5.3$, but if we consider the additional shielding of the O ligands as well as the attractions by the O nuclei, the effective Z probably lies between three and six.

The symmetry group considered here is C_{4v}, and the decomposition of the representation D^l, with $l = 2$, in terms of the C_{4v} irreducible representations $D^2 \rightarrow a_1 + b_1 + b_2 + e$, allows us to label the obtained eigenstates. The axial one $u = |2, 0\rangle$ spans the representation a_1. The electrons, being distributed along the surface normal, avoid the O repulsion. For the doubly degenerate representation e, we use as the basis $\xi = (i/\sqrt{2})[|2, 1\rangle + |2, -1\rangle]$ and $\eta = (-1/\sqrt{2})[|2, 1\rangle - |2, -1\rangle]$ whose lobes point in perpendicular planes above and below the O ions. The third state $\zeta = (-i/\sqrt{2})[|2, 2\rangle - |2, -2\rangle]$ spans the representation b_2, in which the electrons are distributed in a plane parallel to the O ions but rotated by $\frac{1}{4}\pi$ to avoid them. The last state, $v = (1/\sqrt{2})[|2, 2\rangle + |2, -2\rangle]$, has electron density above the O ions, a high energy, and has not been considered. The next step consists in building the three-electron states corresponding to the three 3d electrons of the Cr^{3+} ion. We shall only consider spin quadruplets. Among the two possible ground states which contain the dangling bond u, $(a_1eb_2)^4E$ has a twofold orbital degeneracy and four wavefunctions: $|^4E, \xi, m = \frac{3}{2}\rangle = |u\zeta\xi|$, $|^4E, \xi, m = \frac{1}{2}\rangle = (1/\sqrt{3})[|\bar{u}\zeta\xi| + |u\bar{\zeta}\xi| + |u\zeta\bar{\xi}|]\ldots$ and similarly for $|^4E, \eta\rangle$ by replacing ξ by η, whereas for $(a_1e^2)^4A_2$, $|^4A_2, m = \frac{3}{2}\rangle = |u\xi\eta|\ldots$. When an O ion lies below the metal one, $(e^2b_2)^4B_1$ probably becomes the ground state, with wavefunctions $|^4B_1, m = \frac{3}{2}\rangle = |\xi\eta\zeta|\ldots$.

(A recent calculation of the electronic structure of sapphire can be found in [14] and [15]. Earlier studies are listed in references therein.)

The last step incorporates the H electrons. The H_2 molecule in its ground state $^1\Sigma_g$ is represented by its wavefunction $\psi(^1\Sigma_g) = |g\bar{g}|$ where the Hartree–Fock orbital g is taken as $g = c[\exp(-\lambda r_a) + \exp(-\lambda r_b)]$, where $\lambda = 1.189$ a.u., $c = 0.399$ [16] and r_a (r_b) denotes the distance of the electron from proton a (b). Performing a spherical expansion of the function we shall retain, for numerical applications, the zero-order term of spherical symmetry since it contains about 98% of the total charge. The function g is then given by

$$g = (c/\lambda^2 br)\{[1 + \lambda|r - b|]\exp(-\lambda|r - b|) - [1 + \lambda(r + b)]\exp(-\lambda(r + b))\} \qquad \text{(A1)}$$

where $b = 0.7$ represents half the internuclear distance and r the electron distance from the molecule centre. The overlap integrals $\langle\omega|g\rangle$, where $\omega = \xi, \eta, \zeta, u$ have been computed as a function of the Cr–molecule distance d and of the effective nuclear charge Z. The largest one $\langle u|g\rangle$ is rather important. It has its maximum value at $d = 3$ a.u. and $Z = 2.2$. However below $Z = 3$ this overlap oversteps 0.4, wich requires a different treatment of the molecule–ion electron admixture from that suggested in our model. We consider the five electrons as a whole in the surface–molecule complex and obtain their eigenstates in terms of antisymmetrized products. The molecule and Cr^{3+} ion are considered to be unperturbed in their electron configurations, on account of the weak physisorption, but the effect of antisymmetrization mixes the molecular and ionic characters. Since the molecule and Cr functions are not orthogonal it appears convenient to use, in the following calculations, as an intermediate the first-order orthogonalized Cr eigenfunction. The compound eigenstate for instance $|u\eta\zeta g\bar{g}|$ is clearly invariant by replacing each $\omega = u, \eta, \zeta$ by $|\lambda_\omega\rangle = [|\omega\rangle - |g\rangle\langle g|\omega\rangle][1 - |\langle g|\omega\rangle|^2]^{-1/2}$.

Appendix B. Electron orbital and spin momenta algebra

B.1. The dipolar process

The electron contribution to the dipolar process given by (2.10)

$$K^D(\Gamma) = \frac{12\pi}{5S(S+1)} \sum_{m,m',\gamma,\gamma',\beta} (-)^\beta p_{\gamma,m}\langle \Gamma, \gamma', m'| \times \sum_\alpha E^2_{-\beta}(\alpha)|\Gamma, \gamma, m\rangle\langle \Gamma, \gamma, m| \sum_\alpha E^2_\beta(\alpha)|\Gamma, \gamma', m'\rangle \tag{B1}$$

is calculated by reducing the three-electron matrix elements to one electron ones, transforming the summation over the electrons α in one over the orbitals ω:

$$\langle {}^{2S+1}\Gamma, m| \sum_\alpha E^2_\beta(\alpha)|{}^{2S+1}\Gamma, m'\rangle = \frac{1}{3} \sum_{\omega,\nu} C(312|\beta - \nu, \nu) T^3_{\beta-\nu}(\omega)\langle S, m|S^1_\nu|S, m'\rangle \tag{B2}$$

where we define $T^3(\omega) = \langle \omega|T^3|\omega\rangle$, with ω being one of the orbitals building Γ.

The spin contribution obeys the sum rule

$$\sum_{m,m'} (-)^\nu [S]^{-1}\langle S, m'|S^1_{-\delta}|S, m\rangle\langle S, m|S^1_\nu|S, m'\rangle = \frac{S(S+1)}{3}\delta_{\delta,\nu} \tag{B3}$$

with $[S] = 2S + 1$. By using the following recoupling of Clebsch–Gordan coefficients:

$$C(312|\beta - \nu, \nu)C(312|-\beta + \nu, -\nu) = \sum_k (-)^{\beta+\nu+1}\sqrt{5(2k+1)} \begin{Bmatrix} 2 & 3 & 1 \\ 3 & 2 & k \end{Bmatrix} \times C(33k|-\beta + \nu, \beta - \nu)C(2k2|\beta, 0) \tag{B4}$$

noticing the selection rule $\sum_\beta C(2k2|\beta, 0) = 5\delta_{k,0}$, and recoupling the electron position tensors $\sum_\beta C(33k|\beta, -\beta)T^3_\beta T^3_{-\beta} = [\boldsymbol{T}^3 \times \boldsymbol{T}^3]^k_0$, we obtain for a non-degenerate ground state

$$K^D(\Gamma) = [4\pi/(7 \times 9)]\boldsymbol{T}^3(\Gamma) \cdot \boldsymbol{T}^3(\Gamma) \tag{B5}$$

where $\boldsymbol{T}^3(\Gamma) = \sum_\omega \langle \omega|\boldsymbol{T}^3|\omega\rangle$ sums the different orbital contributions. For ${}^4\Gamma = {}^4B_1$: $\omega = \xi, \eta, \zeta$, while for ${}^4\Gamma = {}^4A_2$, $\omega = u, \xi, \eta$. In the degenerate case, we obtain extra non-diagonal couplings

$$K^D(\Gamma) = [4\pi/(7 \times 9)][\boldsymbol{T}^3(\Gamma) \cdot \boldsymbol{T}^3(\Gamma) + \boldsymbol{T}^3(\gamma, \gamma') \cdot \boldsymbol{T}^3(\gamma', \gamma)] \tag{B6}$$

where we have defined $\boldsymbol{T}^3(\gamma, \gamma') = \langle \gamma|\boldsymbol{T}^3|\gamma'\rangle$. For ${}^4\Gamma = (a_1eb_2){}^4E$, this represents the coupling inside the doubly-degenerate representation e with $(\gamma, \gamma') = (\xi, \eta)$, while ω runs over $u, (\xi, \eta), \zeta$.

B.2. The contact processes

B.2.1. Conversion algebra. The conversion rate can be condensed as a sum of products of electron and nuclei matrix elements as

$$P^{\boldsymbol{Y}}_{o\to p}(\Gamma) = \left(\frac{\lambda_c}{\hbar}\right)^2 J(\omega_{op}) \sum_{h,\gamma\gamma' mm'} p_{\gamma,m} \times \langle p|(\boldsymbol{N}^h \times \boldsymbol{N}^h)^\circ|p\rangle \langle {}^{2S+1}\Gamma, \gamma, m|(\boldsymbol{E}^h \times \boldsymbol{E}^h)^\circ|{}^{2S+1}\Gamma, \gamma, m\rangle. \tag{B7}$$

The nuclear matrix elements are simply worked out:

$$\langle p|(\boldsymbol{N}^h \times \boldsymbol{N}^h)^\circ|p\rangle = \tfrac{1}{3}ab^2(2h+1)^{1/2} \tag{B8}$$

whereas for the electron ones we obtain

$$\langle {}^{2S+1}\Gamma, \gamma, m|(\boldsymbol{E}^h \times \boldsymbol{E}^h)^\circ|{}^{2S+1}\Gamma, \gamma, m\rangle = \sum_g [h]^{1/2}(-)^h \begin{Bmatrix} 1 & 1 & h \\ 1 & 1 & g \end{Bmatrix} \times \langle S, m|(\boldsymbol{S}^1 \times \boldsymbol{S}^1)^g|S, m\rangle \cdot \langle {}^{2S+1}\Gamma, \gamma|(\boldsymbol{\Theta}^1 \times \boldsymbol{\Theta}^1)^g|{}^{2S+1}\Gamma, \gamma\rangle. \tag{B9}$$

The spin matrix elements, being summed over m, lead to the selection rule $g = 0$:

$$\sum_m p_m \langle S, m|(\boldsymbol{S}^1 \times \boldsymbol{S}^1)^g_0|S, m\rangle = -\frac{1}{\sqrt{3}} S(S+1)\delta_{g,0}. \tag{B10}$$

In the case of a non-degenerate orbital ground state Γ, the conversion rate is simply expressed by

$$P^{\boldsymbol{Y}}_{o\to p}(\Gamma) = \tfrac{4}{3}(\lambda_c q_s ab/\hbar)^2 S(S+1) J(\omega_{op}) \boldsymbol{\Theta}^1(\Gamma) \cdot \boldsymbol{\Theta}^1(\Gamma) \tag{B11}$$

which can be written in the form (3.7), provided that we define $K^Y(\Gamma)$ by (3.8).

B.2.2. The orbital form factor. In order to estimate the contact induced transition probability (B11), we calculate the scalar products $\nabla^1\omega \cdot \nabla^1\omega$, which can be expressed in terms of $\nabla^1 R_{3d}Y^2_m \cdot \nabla^1 R_{3d}Y^2_n$. The gradient formula [9] can be written as

$$\nabla^1 R_{3d}Y^2_m = \sum_{i=1,3} \psi_i(r) \boldsymbol{Y}_{2im}$$

where the vector spherical harmonics are defined by $\boldsymbol{Y}_{2im} = [\boldsymbol{Y}^i \times \boldsymbol{e}^1]^2_m$, $\boldsymbol{e}^1$ being the unit tensor and the radial functions ψ being defined by:

$$\psi_1(r) = \sqrt{\tfrac{2}{5}}(\mathrm{d}/\mathrm{d}r + 3/r) R_{3d} = N_{3d}\sqrt{\tfrac{2}{5}}(5r - \tfrac{1}{3}Zr^2)\exp(-\tfrac{1}{3}Zr) \tag{B13}$$

$$\psi_3(r) = -\sqrt{\tfrac{3}{5}}(\mathrm{d}/\mathrm{d}r - 2/r) R_{3d} = N_{3d}\sqrt{\tfrac{3}{5}}(\tfrac{1}{3}Zr^2)\exp(-\tfrac{1}{3}Zr). \tag{B14}$$

After some spherical algebra we obtain

$$\nabla^1 R_{3d}Y^2_m \cdot \nabla^1 R_{3d}Y^2_n = \sum_{ijk} \alpha(ijk) C(22k|mn) \psi_i \psi_j Y^k_{m+n} \tag{B15}$$

where i and j are odd and equal to one or three and k is even and takes the values zero, two and four. We have defined the numerical coefficients

$$\alpha(ijk) = -5\sqrt{\frac{(2i+1)(2j+1)}{4\pi}} \begin{Bmatrix} i & j & k \\ 2 & 2 & 1 \end{Bmatrix} \begin{pmatrix} i & j & k \\ 0 & 0 & 0 \end{pmatrix} \tag{B16}$$

where the large round and curly brackets denote respectively the $3j$ and $6j$ coupling coefficients. If we restrict ourselves now to $m = n = 0$, that is the axial orbital u, and take the molecule at a distance d on the symmetry axis, then (B15) and (B16) give

$$\nabla^1 u(M) \cdot \nabla^1 u(M) = (1/4\pi)[\sqrt{2}\psi_1 - \sqrt{3}\psi_3]^2 \tag{B17}$$

where M denotes the molecule centre. Inserting (B13) and (B14) into (B17), we obtain

$$\nabla^1 u(M) \cdot \nabla^1 u(M) = (2/3^{11}\pi)Z^7 d^2 (Zd - 6)^2 \exp(-\tfrac{2}{3}Zd). \tag{B18}$$

Appendix C. Metal–molecule electron overlap and dipolar matrix elements

We need to obtain matrix elements or the overlap integral with two centres: one at the centre of mass of the H_2 molecule and the other at the metal ion. The shift of the origin and the recoupling of the angular momentum can be made straightforwardly in the Fourier space by using the expansion of the plane wave in terms of the spherical harmonics:

$$\exp(i\boldsymbol{k} \cdot \boldsymbol{r}) = 4\pi \sum_{\ell=0}^{\infty} i^\ell j_\ell(kr) \sum_{m=-\ell}^{\ell} Y_m^\ell(\hat{\boldsymbol{k}})^* Y_m^\ell(\hat{\boldsymbol{r}}) \tag{C1}$$

where $\hat{\boldsymbol{k}}$ and $\hat{\boldsymbol{r}}$ are the direction unit vectors associated with $\boldsymbol{k}$ and $\boldsymbol{r}$ respectively. Then we obtain the overlap integral as

$$\langle g|m\rangle = -32\pi^3\sqrt{\pi} N_g N_{3d} Y_m^2(\hat{\boldsymbol{d}})^* \int_0^\infty \mathrm{d}k\, k^2 \bar{f}_{3d}(k) \bar{f}_{1s}(k) j_0(kb) j_2(kd). \tag{C2}$$

where the Fourier transform of the radial part $f_{1s}(k)$ of the 1s wavefunction of H_2 and the radial part $f_{3d}(k)$ of the 3d wavefunction are given by

$$\bar{f}_{1s}(k) = (\lambda/2\pi^2)\mathcal{D}_\lambda/(k^2 + \lambda^2) \tag{C3}$$

$$\bar{f}_{3d}(k) = -(\kappa/2\pi^2)\mathcal{D}_\kappa^3(k^2/k^2 + \kappa^2) \tag{C4}$$

with $\kappa = \frac{1}{3}Z$, λ as defined above (A1) and the following definition of $\mathcal{D}_x^n$:

$$\mathcal{D}_x^n = [-(1/x)\partial/\partial x]^n. \tag{C5}$$

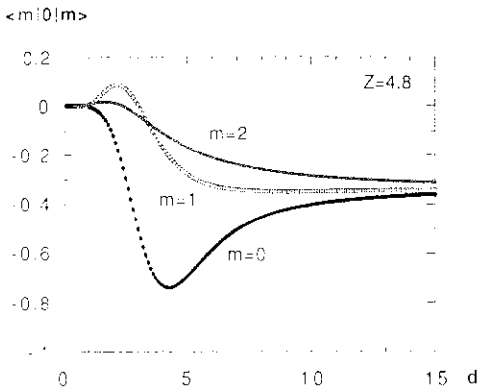

Figure C1. The matrix elements $\langle m|0|n\rangle$, defined in the text, are represented as a function of the Cr–molecule distance d, for $Z = 4.8$.

Table C1. List of the functions F.

L	ℓ	$F(z; L, \ell)$
0	3	$3\times 5(z/(3\times 5\times 6!)+1/(3\times 5\times 6!)-z^{-7}[\exp z-\sum_{n=0}^{6} z^n/n!])\exp(-z)$
2	5	$(7\times 9!/6!)[3/(7\times 10!)]z--z^{-9}[\exp z-\sum_{n=0}^{10} z^n/n!]\exp(-z)$
2	3	$(1/6!)(z-2)\exp(-z)$
2	1	$(1/6!)(z-7)\exp(-z)$
4	7	$-[(13\times 11!)/6!](1/13!)z+z^{-11}[\exp z-\sum_{n=0}^{12} z^n/n!]\exp(-z)$
4	5	$(1/6!)z\exp(-z)$
4	3	$(1/6!)(z-9)\exp(-z)$
4	1	$(1/6!)(z-14+35z^{-1}+35z^{-2})\exp(-z)$

Table C2. List of the coefficients C.

m	L	ℓ	$C_m(L,\ell)$	m	L	ℓ	$C_m(L,\ell)$
0	0	3	$1/3^2\times 5$	2	0	3	$1/3^2\times 5$
	2	5	$2^2\times 5/3^3\times 7^2$		2	5	$-2^2\times 5/3^3\times 7^2$
	2	3	$2^3/3^3\times 5\times 7$		2	3	$-2^3/3^3\times 5\times 7$
	2	1	$2/5\times 7^2$		2	1	$-2/5\times 7^2$
	4	7	$2\times 5/3\times 11\times 13$		4	7	$5/3^2\times 11\times 13$
	4	5	$2^3/7^2\times 13$		4	5	$2^2/3\times 7^2\times 13$
	4	3	$2^2/5\times 7\times 11$		4	3	$2/3\times 5\times 7\times 11$
	4	1	$2^3/3\times 5\times 7^2$		4	1	$2^2/3^2\times 5\times 7^2$
1	0	3	$1/3^2\times 5$	nd	0	3	0
	2	5	$2\times 5/3^3\times 7^2$		2	5	$-2^{1/2}\times 5^{1/2}/3^{5/2}\times 7^2$
	2	3	$2^2/3^3\times 5\times 7$		2	3	$2^{3/2}/3^{5/2}\times 5^{1/2}\times 7$
	2	1	$1/5\times 7^2$		2	1	$-2^{1/2}/3^{1/2}\times 5^{1/2}\times 7^2$
	4	7	$-2^2\times 5/3^2\times 11\times 13$		4	7	$-2^{3/2}\times 5^{1/2}/3^{3/2}\times 11\times 13$
	4	5	$-2^4/3\times 7^2\times 13$		4	5	$2^{9/2}\times 5^{1/2}/3^{3/2}\times 7^2\times 13$
	4	3	$-2^3/3\times 5\times 7\times 11$		4	3	$2^{3/2}/3^{3/2}\times 5^{1/2}\times 7\times 11$
	4	1	$-2^4/3^2\times 5\times 7^2$		4	1	$-2^{5/2}/3^{3/2}\times 5^{1/2}\times 7^2$

The dipole matrix elements $\langle R_{3d}Y_m^2|T_\alpha^3|R_{3d}Y_n^2\rangle \equiv \langle m|\alpha|n\rangle$ are also calculated along the same line. We shift the origin of coordinates for T_α^3. The general expression is given as

$$\langle m|\alpha|n\rangle = -(4\pi)^2 N_{3d}^2 \sum_{L,\ell} i^{L+\ell} Y_{m-n-\alpha}^{\ell}(\hat{d})^* C_Y(\ell, 3, L; m-n-\alpha, \alpha) C_Y(2, L, 2; n, m-n)$$

$$\times \int_0^\infty dk\, k^2 \mathcal{T}^3(k) j_\ell(kd) \int_0^\infty dr\, r^2 R_{3d}(r)^2 j_L(kr). \tag{C6}$$

Here the radial part of the Fourier transform of $T^3(r)$, denoted $\mathcal{T}^3(k)$, is given by

$$\mathcal{T}^3(k) = ik/30\pi. \tag{C7}$$

The coupling constant C_Y is given in terms of the Clebsh–Gordan coefficients as

$$C_Y(\ell_1, \ell_2, \ell|m_1, m_2) = \sqrt{(2\ell_1+1)(2\ell_2+1)/4\pi(2\ell+1)}$$

$$\times C(\ell_1, \ell_2, \ell|m_1, m_2) C(\ell_1, \ell_2, \ell|0, 0). \tag{C8}$$

Noticing that the spherical Bessel function $j_\ell(x)$ satisfies

$$j_\ell(x) = x^\ell \mathcal{D}_x^\ell j_0(x) = x^\ell \mathcal{D}_x^\ell (\sin x/x) \tag{C9}$$

we obtain

$$\langle m|\alpha|n\rangle = \frac{\pi \nu^7}{2^2 \times 3^3 \times 5^2} \sum_{L,\ell} Y_{m-n-\alpha}^{\ell}(\hat{d})^* C(\ell, 3, L; m-n-\alpha, n) C(2, L, 2; n, m-n)$$

$$\times (-\partial_\nu)^{5-L} \mathcal{D}_\nu^L d^\ell \mathcal{D}_d^\ell \frac{1}{d} \left[\nu^{1+L-\ell} \exp(-\nu d) - \frac{1}{\nu^2} \delta_{\ell-L,3} \right] \tag{C10}$$

where $\nu = 2\kappa = \frac{2}{3}Z$. It is worthwhile noticing here that we obtain power law terms, not only the Wigner term but additional power terms, as well as exponential decreases.

When the molecule is located on the axis of symmetry as assumed in the text, we have the selection rule

$$m = n + \alpha. \tag{C11}$$

After lengthy calculations for the differentiation in (C10), we obtain

$$\langle m|0|m\rangle = A d^{-4} z^7 \sum_{L,\ell} C_m(L, \ell) F(z; L, \ell) \tag{C12}$$

$$\langle 1|2|-1\rangle = A d^{-4} z^7 \sum_{L,\ell} C_{nd}(L, \ell) F(z; L, \ell) \tag{C13}$$

where $z = \nu d = \frac{2}{3} Z d$. The functions F and coefficients C are listed, for allowed values of L and ℓ, in tables C1 and C2. In figure C1, we show $\langle m|0|m\rangle$ as a function of the distance d.

References

[1] Wigner E 1933 *Z. Phys. Chem.* B **23** 28
[2] Ilisca E 1992 *Prog. Surf. Sci.* **41** 217
[3] Selwood P W 1966 *J. Am. Chem. Soc.* **88** 2676
[4] Ashmead D R, Eley D D and Rudham R 1964 *J. Catal.* **3** 280
[5] King J and Benson S 1966 *J. Chem. Phys.* **44** 1007
[6] Sugano S, Tanabe T and Kamimura H 1970 *Multiplets of Transition Metal Ions in Crystals* (New York: Academic)
[7] Ilisca E and Legrand A P 1972 *Phys. Rev.* B **5** 4994
[8] Petzinger K G and Scalapino D J 1973 *Phys. Rev.* B **8** 266
[9] Edmonds A R 1974 *Angular Momentum in Quantum Mechanics* (Princeton, NJ: Princeton University Press)
[10] Ilisca E 1990 *Chem. Phys. Letters* **168** 289
[11] Buckingham A D and Kollman P A 1972 *Mol. Phys.* **23** 65
[12] Ilisca E and Sugano S 1986 *Phys. Rev. Lett.* **57** 2590
[13] Coulson C A 1979 *Valence* (Oxford: Oxford University Press)
[14] Guo J, Ellis D E and Lam D J 1992 *Phys. Rev.* B **45** 3204
[15] Guo J, Ellis D E and Lam D J 1992 *Phys. Rev.* B **45** 13647
[16] Cade P E and Wahl A C 1974 *At. Data Nucl. Data Tables* **13** 339